Nuclear Instruments and Methods 215 (1983) 147-157
North-Holland Publishing Company

PROTON-CARBON EFFECTIVE ANALYZING POWER BETWEEN 95 AND 570 MeV

E. APRILE-GIBONI, R. HAUSAMMANN *, E. HEER, R. HESS, C. LECHANOINE-LE LUC, W. LEO, S. MORENZONI, Y. ONEL and D. RAPIN

DPNC, University of Geneva, CH-1211 Geneva, Switzerland

Received 21 January 1983

The p-C effective analyzing power has been measured with a good accuracy for laboratory scattering angles between 5° and 20° at 25 energies from 95 to 570 MeV. Carbon targets from 3 to 7 cm have been used. Measurements have been made at SIN with multiwire proportional chambers. A smooth angle and energy depending function has been fitted to the data. Reasonable agreement has been found with other available data.

1. Introduction

In order to determine the spin dependence of the nuclear interaction, measurements of the polarization of particles in their final state is often required. At intermediate energies (100 MeV to 1 GeV), the measured asymmetry resulting from a second scattering is widely used. The polarization of the particles can be extracted provided the analyzing power A_c of the second scattering is known.

We present here the calibration measurement of a carbon polarimeter for protons used at SIN in the p-p elastic scattering program. These measurements have allowed us to determine completely the scattering matrix [1,2] by the mean of the measurement of 2- and 3-spin observables [2,3].

* Present address: Physics Department, University of California at Irvine, Ca 92717, USA.

2. Apparatus

The SIN PM1 proton beam line was used in its parasitic mode. This beam is produced by the elastic scattering of the 590 MeV unpolarized beam on a beryllium target at 8° laboratory angle. The resulting beam polarization is $P_B = 0.4165 \pm 0.0043$ as shown in ref. 4. A variable thickness copper degrader is used to lower the beam energy. Depolarization effects are negligible since particles are collected at zero degree after the degrader within a small solid angle and because the Coulomb interaction is dominant at these angles. Finally a superconducting solenoid allows a rotation of the beam polarization within the transversal plane up to 180°.

Fig. 1. shows a scale drawing of the polarimeter. It consists of a variable length carbon target sandwiched by multiwire proportional chambers (MWPC) with 2 mm wire spacing. The incoming and outgoing tracks are detected by two telescopes consisting of 3 (respectively 4) x-y MWPCs. A scintillator (Z) placed into the first telescope is used to detect an incoming particle.

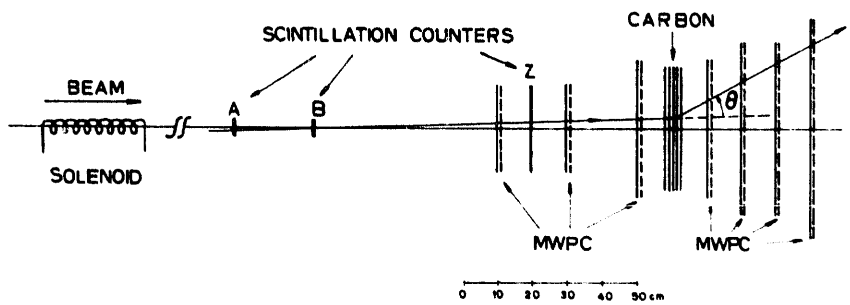

Fig. 1. Scale drawing of the apparatus.

The polarimeter is mounted on a turntable and was placed directly into the beam for the present measurement. Two beam counters A and B were also added. No counters were used behind the carbon target.

3. Data acquisition system

A first level trigger was made with the coincidence between the A, B and Z counters. This opened the gate of the wire memories and initiated the MWPC coding system operations.

A second level hardware trigger, connected to the MWPC logic, was used to reduce the amount of data [5]. The slopes of the particle trajectories and the resulting scattering angle were then computed. Events without significant scattering were rejected. Configurations which were impossible to reconstruct in a further processing were also rejected. 90–95% of the events were rejected. The duration of this decision was about 3.5 μs.

Events having passed this filter were then transfered to DPNC 811 minicomputers [6] under the control of a PDP 11/20. The minicomputers fully reconstructed the events and accumulated event statistics and histograms. Only sums were recorded onto magnetic tapes.

4. Measurements

The geometrical position of the MWPC's were measured on-line using unscattered events taken without the carbon target.

Twenty-five measurements were made at various energies with a 3, 5 or 7 cm thick carbon target. The 3 cm target was used mainly at low energies. For each measurement at least two datasets were taken with opposite beam polarization directions. Some of these were taken with 4 orientations: up, down, left and right.

During these measurements the operational conditions of the 2nd level trigger were changed in order to accept some unscattered data for a check of the geometry. These data were used to monitor possible residual misalignments and allowed an off-line correction of the asymmetries. An estimation of the angular resolution of the apparatus was also possible with these data.

5. Analysis

5.1. General formalism

Consider an incident proton beam propagating along the $\hat{k}$ direction with a transverse polarization vector $\boldsymbol{P}_B$ described by

$$\boldsymbol{P}_B = P_x \cdot \hat{X} + P_y \cdot \hat{Y}.$$

Let $\hat{k}$ and $\hat{k}'$ be unit vectors along the trajectories entering and leaving the carbon. For the scattering in a plane whose normal vector is given by

$$\hat{n} = \hat{k} \times \hat{k}' / |\hat{k} \times \hat{k}'|,$$

the polar θ and azimuthal ϕ scattering angles are defined by

$$\sin\theta = |\hat{k} \times \hat{k}'|, \quad \sin\phi = -\hat{X}\cdot\hat{n}, \quad \cos\phi = \hat{Y}\cdot\hat{n}.$$

The polarized cross section $I(\theta,\phi)$ is expressed by

$$\begin{aligned} I(\theta,\phi) &= I_0(\theta)[1 + A_c(\theta)\boldsymbol{P}_B\cdot\hat{n}] \\ &= I_0(\theta)[1 + P_y A_c(\theta)\cos\phi - P_x A_c(\theta)\sin\phi] \\ &= I_0(\theta)[1 + \epsilon_n(\theta)\cos\phi + \epsilon_s(\theta)\sin\phi], \end{aligned}$$

where $I_0(\theta)$ is the unpolarized cross section, $A_c(\theta)$ the carbon analyzing power and ϵ_n, ϵ_s the asymmetries. These asymmetries can be obtained by a statistical analysis of the azimuthal distribution. Knowledge of $\boldsymbol{P}_B$ allows extraction of A_C.

A relative misalignment of the detectors produces errors in the reconstructed scattering angles θ and ϕ:

$$\Delta\theta_x = \Delta(\mathrm{tg}\theta\cdot\sin\phi), \qquad \Delta\theta_y = \Delta(\mathrm{tg}\theta\cdot\cos\phi).$$

As shown in ref. 7, the effects on the measured asymmetries are

$$\Delta\epsilon_n = \Delta\theta_y \frac{\mathrm{d}}{\mathrm{d}\theta}(\log I_0),$$

$$\Delta\epsilon_s = \Delta\theta_x \frac{\mathrm{d}}{\mathrm{d}\theta}(\log I_0),$$

if the misalignments $\Delta\theta_x$ and $\Delta\theta_y$ are small.

These effects can hence be corrected if $I_0(\theta)$, $\Delta\theta_x$ and $\Delta\theta_y$ are known.

5.2. On-line analysis

Events accepted by the 2nd level trigger were transferred to minicomputers for reconstruction. The raw coordinates were first corrected for the geometrical displacements of the MWPC's from their nominal positions. Events were then fully reconstructed and tested for the following requirements:

1) MWPC track alignment of the incoming and outgoing trajectories. The S^2 per degree of freedom was requested to be less than 4 mm^2.
2) Projection of the incoming track into the last backward chamber in order to guarantee a 100% geometrical acceptance.
3) The distance of closest approach between incoming and outgoing tracks. This had to be less than 4 mm.
4) The reconstructed longitudinal position of the carbon vertex was required to fall within the target with an accuracy of ± 27 mm.
5) Range of θ between 5° and 20°.

Cuts (1) to (4) eliminated mainly events scattered on the counters or the MWPCs which were accepted by the

2nd level trigger. From 6 to 11% of the processed events were rejected mainly by cut (1), while 40 to 50% of the remaining events were rejected by cut (5) mainly because of a too small scattering angle. Accepted events were finally accumulated in a two dimensional histogram divided into 15 bins for θ and 16 bins for ϕ.

Processing of the unscattered events differed slightly. No vertex was computed and a cut was applied on θ whose maximum value depends on energy and target length. Sums were accumulated in order to evaluate the mean and the width of the distribution of the projected angles $\mathrm{tg}\theta \cdot \cos\phi$ and $\mathrm{tg}\theta \cdot \sin\phi$.

5.3. Off-line analysis

The analysis was facilitated by the 100% geometrical acceptance. The asymmetries were extracted at each polar angle θ by a simple Fourier analysis of the ϕ distributions obtained from the two dimensional histograms. The effect of the bin width in ϕ was also taken into account. The angular dependence of the unpolarized inclusive cross section was also obtained from these histograms.

The residual misalignments were found to be less than 0.02°. The corresponding corrections have been applied on the asymmetries. They were of the order of 0.004 and smaller than the statistical errors.

The analyzing power A_c was extracted for each beam polarization orientation. The data are very consistent as shown in table 1. These have been consequently summed over the different orientations. This operation generally cancels the effects of the misalignment corrections.

6. Results

The experimental results for the effective proton carbon analyzing power A_c are shown in table 1 and in fig. 2. A_c is maximum around 200 MeV and decreases rapidly at low energies. The inclusive differential cross section $(\mathrm{d}\sigma/\mathrm{d}\Omega)$ results can be seen in table 1. The cross section values are in arbitrary units. Quoted errors are purely statistical. The A_c results are subject to an overall normalization uncertainty of 1% coming from the beam polarization. The given kinetic beam energies are computed at the center of the target.

The target thickness was found to have no visible effect above 270 MeV. At lower energies and at larger angles however, the 7 cm data shows an higher analyzing power than the 3 cm data. This can be understood by considering the amount of inelastic events accepted by the apparatus. Since low energy particles cannot escape from a thick target, the length of the target acts as an inelasticity limiter. The 3 cm target allows a larger amount of inelasticities and the effective analyzing power is thus reduced.

At low energies A_c drops rapidly to zero at small angles. This is due to multiple Coulomb scattering which extends up to our measured angles. This effect is of course very dependent on the target length.

7. Energy dependent fits

A parametrization of A_c was necessary for the pp elastic scattering data analysis [3] where the carbon analyzing power was needed for continuously variable kinematic conditions. We have performed an angle and energy dependent smoothing by adjusting the following empirical formula to our experimental data:

$$A_c(\theta, T) = D(\theta, T)\alpha(T) \times \left[\frac{\sin\theta}{1 + \beta(T)\sin^2\theta + \gamma(T)\sin^4\theta} + \delta(T)\sin\theta \right].$$

This expression is similar to the one suggested in ref. 8 but two extra terms $\delta(T)$ and $D(\theta, T)$ have been added. α, β, γ and δ are energy dependent polynomials of the form:

$$\alpha(T) = \alpha_0 + \alpha_1 X + \alpha_2 X^2 + \alpha_3 X^3 + \alpha_4 X^4,$$

where $X = (T - T_{\mathrm{central}})/T_{\mathrm{range}}$ is a dimensionless energy variable depending on the region where the fit is applied.

$D(\theta, T)$ is an empirical damping factor used to reproduce the sharp drop of A_c toward small angles induced by multiple Coulomb scattering at low energies. This can be expressed as:

$$D(\theta, T) = \frac{1}{1 + C\exp\left[\theta^2/2\theta_s^2(T)\right]}.$$

The term $\theta_s^2(T) = C_0 + C_1(15/p\beta)^2$ is an attempt to describe the angular resolution as the sum of the constant MWPC resolution plus a momentum dependent multiple scattering term. C_0 has been fixed to the measured value of the MWPCs resolution extrapolated to $T \to \infty$. C and C_1 are free parameters, the $15/p\beta$ term being expressed in degrees.

Since the target length has a non negligible influence at low energies, it was not possible to fit all the data over the entire energy range. To facilitate the analysis of the pp experiment [3], two separate fits were made:

(1) A high energy fit (denoted by "H") valid for 7 cm target from 150 to 571 MeV. This contains all the present 7 cm data, 5 cm data above 270 MeV and 3 cm data above 300 MeV. Data from our previous experiment (SIN – DRAP, ref. 7), taken with the same beam and with a similar apparatus above 299 MeV, were also included.

Table 1
Proton–carbon effective analyzing power and differential cross-section. Cross-section data are in arbitrary units.

Energy	151 ± 3 MeV	179 ± 3 MeV	215 ± 2 MeV	225 ± 2 MeV	269 ± 2 MeV	300 ± 2 MeV	345 ± 2 MeV	384 ± 2 MeV	427 ± 2 MeV
Target length	7 cm 12.40 g/cm^2	7 cm 12.40 g/cm^2	7 cm 12.40 g/cm^2	7 cm 12.40 g/cm^2	7 cm 12.40 g/cm^2	7 cm 12.40 g/cm^2	7 cm 12.40 g/cm^2	7 cm 12.40 g/cm^2	7 cm 12.40 g/cm^2
Angular resolution	1.315°		1.043°			0.753°	0.684°	0.645°	0.595°
Up–down consistency [χ^2/df]	1.740	1.092	0.929	1.383	1.332	1.087	0.869	1.688	1.152
θ[°]	A_c	A_c	A_c	A_c	A_c	A_c	A_c	A_c	A_c
5.5	0.156 ± 0.011	0.282 ± 0.016	0.355 ± 0.013	0.330 ± 0.017	0.385 ± 0.015	0.395 ± 0.016	0.365 ± 0.010	0.356 ± 0.015	0.326 ± 0.011
6.5	0.269 ± 0.015	0.414 ± 0.017	0.445 ± 0.013	0.444 ± 0.017	0.451 ± 0.015	0.450 ± 0.015	0.423 ± 0.010	0.415 ± 0.015	0.393 ± 0.011
7.5	0.368 ± 0.015	0.426 ± 0.016	0.493 ± 0.012	0.501 ± 0.017	0.487 ± 0.015	0.510 ± 0.015	0.466 ± 0.010	0.439 ± 0.015	0.399 ± 0.011
8.5	0.420 ± 0.014	0.464 ± 0.016	0.522 ± 0.012	0.522 ± 0.016	0.559 ± 0.015	0.548 ± 0.016	0.511 ± 0.010	0.447 ± 0.016	0.405 ± 0.012
9.5	0.425 ± 0.014	0.503 ± 0.016	0.575 ± 0.012	0.610 ± 0.016	0.570 ± 0.015	0.581 ± 0.016	0.484 ± 0.011	0.436 ± 0.016	0.391 ± 0.013
10.5	0.422 ± 0.014	0.537 ± 0.016	0.588 ± 0.013	0.627 ± 0.017	0.554 ± 0.016	0.564 ± 0.017	0.483 ± 0.011	0.435 ± 0.017	0.384 ± 0.013
11.5	0.426 ± 0.014	0.547 ± 0.016	0.618 ± 0.013	0.600 ± 0.017	0.571 ± 0.016	0.533 ± 0.017	0.478 ± 0.012	0.407 ± 0.018	0.355 ± 0.014
12.5	0.461 ± 0.014	0.587 ± 0.017	0.625 ± 0.013	0.620 ± 0.018	0.584 ± 0.017	0.524 ± 0.018	0.442 ± 0.012	0.391 ± 0.019	0.348 ± 0.015
13.5	0.511 ± 0.015	0.590 ± 0.017	0.596 ± 0.014	0.604 ± 0.019	0.528 ± 0.018	0.491 ± 0.019	0.387 ± 0.013	0.343 ± 0.020	0.284 ± 0.016
14.5	0.531 ± 0.015	0.563 ± 0.018	0.602 ± 0.015	0.597 ± 0.020	0.476 ± 0.018	0.411 ± 0.019	0.348 ± 0.013	0.279 ± 0.021	0.271 ± 0.016
15.5	0.484 ± 0.016	0.588 ± 0.019	0.581 ± 0.015	0.567 ± 0.020	0.443 ± 0.019	0.383 ± 0.020	0.317 ± 0.014	0.260 ± 0.021	0.252 ± 0.016
16.5	0.524 ± 0.017	0.587 ± 0.020	0.539 ± 0.016	0.486 ± 0.021	0.391 ± 0.019	0.330 ± 0.021	0.281 ± 0.014	0.204 ± 0.021	0.211 ± 0.016
17.5	0.537 ± 0.017	0.554 ± 0.020	0.494 ± 0.016	0.456 ± 0.021	0.330 ± 0.020	0.329 ± 0.021	0.239 ± 0.014	0.217 ± 0.022	0.203 ± 0.016
18.5	0.525 ± 0.018	0.533 ± 0.021	0.423 ± 0.016	0.421 ± 0.022	0.286 ± 0.020	0.260 ± 0.021	0.224 ± 0.014	0.227 ± 0.021	0.208 ± 0.016
19.5	0.512 ± 0.019	0.454 ± 0.022	0.376 ± 0.017	0.356 ± 0.022	0.254 ± 0.020	0.243 ± 0.021	0.238 ± 0.014	0.173 ± 0.022	0.192 ± 0.016
δ_{exp} Data/Fit (L) Data/Fit (H)	0.992 ± 0.009	1.002 ± 0.009	1.010 ± 0.007	1.012 ± 0.009	0.987 ± 0.009	1.020 ± 0.010	0.997 ± 0.007	0.992 ± 0.012	1.002 ± 0.011
θ[°]	$d\sigma/d\Omega$	$d\sigma/d\Omega$	$d\sigma/d\Omega$	$d\sigma/d\Omega$	$d\sigma/d\Omega$	$d\sigma/d\Omega$	$d\sigma/d\Omega$	$d\sigma/\Omega$	$d\sigma/\Omega$
5.5	100.00 ± 0.33	100.00 ± 0.47	100.00 ± 0.38	100.00 ± 0.49	100.00 ± 0.45	100.00 ± 0.46	100.00 ± 0.29	100.00 ± 0.43	100.00 ± 0.32
6.5	51.69 ± 0.22	75.72 ± 0.37	84.92 ± 0.32	86.52 ± 0.42	87.39 ± 0.38	87.07 ± 0.39	85.60 ± 0.25	84.61 ± 0.37	83.58 ± 0.27
7.5	44.02 ± 0.19	69.26 ± 0.33	77.15 ± 0.28	77.95 ± 0.37	75.91 ± 0.33	75.25 ± 0.34	72.41 ± 0.21	70.06 ± 0.31	68.20 ± 0.23
8.5	41.35 ± 0.17	63.88 ± 0.30	69.47 ± 0.25	69.39 ± 0.33	66.43 ± 0.29	63.73 ± 0.29	60.20 ± 0.18	57.28 ± 0.26	54.62 ± 0.19
9.5	38.49 ± 0.16	58.42 ± 0.27	61.74 ± 0.23	61.51 ± 0.29	56.66 ± 0.26	54.55 ± 0.26	50.18 ± 0.16	46.23 ± 0.22	44.00 ± 0.16
10.5	35.74 ± 0.15	51.60 ± 0.24	54.19 ± 0.20	53.32 ± 0.26	47.84 ± 0.22	45.74 ± 0.22	41.80 ± 0.14	38.22 ± 0.19	34.93 ± 0.14
11.5	32.20 ± 0.13	45.72 ± 0.22	46.62 ± 0.18	45.55 ± 0.23	40.80 ± 0.20	38.79 ± 0.20	34.46 ± 0.12	31.26 ± 0.17	28.43 ± 0.12
12.5	28.39 ± 0.12	39.53 ± 0.20	40.32 ± 0.16	39.02 ± 0.20	34.74 ± 0.17	32.71 ± 0.17	28.91 ± 0.10	25.98 ± 0.15	23.68 ± 0.10
13.5	24.66 ± 0.11	34.16 ± 0.17	34.58 ± 0.14	34.05 ± 0.18	29.86 ± 0.16	28.03 ± 0.16	24.53 ± 0.09	22.45 ± 0.13	20.19 ± 0.09
14.5	21.21 ± 0.10	29.26 ± 0.16	29.43 ± 0.13	28.90 ± 0.16	25.73 ± 0.14	24.35 ± 0.14	21.37 ± 0.08	19.23 ± 0.12	17.62 ± 0.08
15.5	18.19 ± 0.09	25.23 ± 0.14	25.84 ± 0.12	25.28 ± 0.15	23.01 ± 0.13	21.35 ± 0.13	19.21 ± 0.08	17.55 ± 0.11	16.13 ± 0.08
16.5	15.69 ± 0.08	21.90 ± 0.13	22.83 ± 0.11	22.57 ± 0.13	20.65 ± 0.12	19.39 ± 0.12	17.60 ± 0.07	16.04 ± 0.10	15.01 ± 0.07
17.5	13.30 ± 0.07	19.24 ± 0.12	20.40 ± 0.10	20.49 ± 0.12	18.84 ± 0.11	17.84 ± 0.11	16.27 ± 0.07	14.98 ± 0.09	14.10 ± 0.07
18.5	11.41 ± 0.06	16.95 ± 0.11	18.43 ± 0.09	18.48 ± 0.12	17.56 ± 0.10	16.90 ± 0.10	15.20 ± 0.06	14.38 ± 0.09	13.46 ± 0.06
19.5	9.78 ± 0.06	14.99 ± 0.10	16.96 ± 0.08	17.16 ± 0.11	16.21 ± 0.10	15.89 ± 0.10	14.68 ± 0.06	13.51 ± 0.09	12.77 ± 0.06
No. of events	782011	564131	903712	538507	604003	551495	1252522	534953	919093

Table 1 (continued)

Energy	434 ± 2 MeV	475 ± 2 MeV	520 ± 2 MeV	568 ± 2 MeV	187 ± 3 MeV	275 ± 2 MeV	350 ± 2 MeV	571 ± 2 MeV
Target length	7 cm 12.40 g/cm^2	7 cm 12.40 g/cm^2	7 cm 12.40 g/cm^2	7 cm 12.40 g/cm^2	5 cm 8.85 g/cm^2	5 cm 8.85 g/cm^2	5 cm 8.85 g/cm^2	5 cm 8.85 g/cm^2
Angular resolution	0.597°	0.557°	0.526°	0.515°		0.701°	0.603°	0.476°
Up–down consistency $[\chi^2/df]$	1.512	1.308	1.353	0.870	0.596	1.431	0.746	0.794
θ[°]	A_c	A_c	A_c	A_c	A_c	A_c	A_c	A_c
5.5		0.283 ± 0.011	0.298 ± 0.011	0.295 ± 0.014	0.293 ± 0.017	0.372 ± 0.016	0.349 ± 0.015	0.299 ± 0.014
6.5		0.367 ± 0.011	0.330 ± 0.012	0.302 ± 0.015	0.431 ± 0.017	0.452 ± 0.016	0.419 ± 0.015	0.321 ± 0.014
7.5	0.383 ± 0.014	0.363 ± 0.011	0.323 ± 0.012	0.333 ± 0.016	0.435 ± 0.017	0.481 ± 0.016	0.489 ± 0.015	0.340 ± 0.015
8.5	0.394 ± 0.015	0.386 ± 0.012	0.339 ± 0.013	0.319 ± 0.017	0.498 ± 0.016	0.540 ± 0.016	0.472 ± 0.016	0.311 ± 0.016
9.5	0.403 ± 0.016	0.386 ± 0.013	0.339 ± 0.014	0.299 ± 0.018	0.506 ± 0.016	0.524 ± 0.016	0.486 ± 0.016	0.321 ± 0.018
10.5	0.342 ± 0.017	0.324 ± 0.014	0.313 ± 0.015	0.272 ± 0.020	0.527 ± 0.016	0.589 ± 0.016	0.489 ± 0.017	0.263 ± 0.019
11.5	0.353 ± 0.018	0.336 ± 0.014	0.241 ± 0.016	0.218 ± 0.021	0.575 ± 0.017	0.573 ± 0.017	0.450 ± 0.018	0.257 ± 0.020
12.5	0.307 ± 0.019	0.259 ± 0.015	0.238 ± 0.017	0.226 ± 0.022	0.591 ± 0.017	0.541 ± 0.018	0.394 ± 0.019	0.258 ± 0.021
13.5	0.278 ± 0.020	0.232 ± 0.016	0.212 ± 0.018	0.249 ± 0.022	0.619 ± 0.018	0.530 ± 0.019	0.359 ± 0.020	0.219 ± 0.022
14.5	0.239 ± 0.020	0.240 ± 0.016	0.212 ± 0.018	0.191 ± 0.022	0.579 ± 0.018	0.465 ± 0.019	0.338 ± 0.020	0.180 ± 0.022
15.5	0.241 ± 0.021	0.249 ± 0.016	0.227 ± 0.018	0.227 ± 0.022	0.567 ± 0.019	0.380 ± 0.020	0.275 ± 0.021	0.201 ± 0.022
16.5	0.228 ± 0.021	0.224 ± 0.016	0.208 ± 0.018	0.236 ± 0.022	0.568 ± 0.020	0.356 ± 0.020	0.283 ± 0.021	0.218 ± 0.022
17.5	0.184 ± 0.021	0.174 ± 0.016	0.219 ± 0.018	0.198 ± 0.022	0.524 ± 0.021	0.312 ± 0.021	0.255 ± 0.021	0.190 ± 0.022
18.5	0.204 ± 0.021	0.189 ± 0.016	0.189 ± 0.018	0.186 ± 0.023	0.454 ± 0.021	0.284 ± 0.021	0.217 ± 0.021	0.228 ± 0.022
19.5	0.215 ± 0.021	0.202 ± 0.016	0.190 ± 0.018	0.177 ± 0.023	0.442 ± 0.022	0.255 ± 0.021	0.218 ± 0.021	0.189 ± 0.023
δ_{exp} Data/fit (L) Data/fit (H)	0.982 ± 0.016	1.012 ± 0.012	0.993 ± 0.014	0.993 ± 0.018		0.971 ± 0.009	0.982 ± 0.012	1.018 ± 0.018
θ[°]	$d\sigma/d\Omega$	$d\sigma/d\Omega$	$d\sigma/d\Omega$	$d\sigma/d\Omega$	$d\sigma/d\Omega$	$d\sigma/d\Omega$	$d\sigma/d\Omega$	$d\sigma/d\Omega$
5.5	100.00 ± 0.40	100.00 ± 0.31	100.00 ± 0.33	100.00 ± 0.41	100.00 ± 0.51	100.00 ± 0.47	100.00 ± 0.45	100.00 ± 0.40
6.5	83.13 ± 0.34	81.96 ± 0.26	80.06 ± 0.27	78.03 ± 0.33	87.87 ± 0.44	87.21 ± 0.40	86.08 ± 0.38	77.28 ± 0.32
7.5	67.55 ± 0.29	64.20 ± 0.21	61.69 ± 0.22	58.47 ± 0.27	80.96 ± 0.40	76.57 ± 0.35	72.56 ± 0.33	58.62 ± 0.26
8.5	53.53 ± 0.24	50.44 ± 0.18	47.86 ± 0.18	44.74 ± 0.22	73.89 ± 0.35	65.71 ± 0.31	60.15 ± 0.28	43.72 ± 0.21
9.5	43.00 ± 0.20	39.89 ± 0.15	36.66 ± 0.15	34.15 ± 0.18	67.05 ± 0.32	56.58 ± 0.27	50.31 ± 0.24	33.06 ± 0.17
10.5	34.16 ± 0.17	31.29 ± 0.13	28.71 ± 0.13	26.57 ± 0.15	59.88 ± 0.29	48.18 ± 0.24	41.42 ± 0.21	25.70 ± 0.15
11.5	27.73 ± 0.15	25.46 ± 0.11	23.05 ± 0.11	21.65 ± 0.13	52.56 ± 0.26	40.61 ± 0.21	34.41 ± 0.18	20.92 ± 0.13
12.5	23.09 ± 0.13	20.98 ± 0.09	19.46 ± 0.10	18.51 ± 0.12	45.37 ± 0.23	34.61 ± 0.18	28.84 ± 0.16	17.82 ± 0.11
13.5	19.97 ± 0.12	18.19 ± 0.08	16.98 ± 0.09	16.57 ± 0.11	39.50 ± 0.21	29.77 ± 0.16	24.33 ± 0.14	15.90 ± 0.10
14.5	17.62 ± 0.11	16.36 ± 0.08	15.34 ± 0.08	15.02 ± 0.10	33.59 ± 0.18	26.02 ± 0.15	21.26 ± 0.13	14.54 ± 0.09
15.5	16.03 ± 0.10	14.87 ± 0.07	14.24 ± 0.07	13.95 ± 0.09	29.52 ± 0.17	22.83 ± 0.13	18.93 ± 0.12	13.59 ± 0.09
16.5	15.05 ± 0.09	13.95 ± 0.07	13.35 ± 0.07	13.10 ± 0.09	25.73 ± 0.15	20.69 ± 0.12	17.42 ± 0.11	12.69 ± 0.08
17.5	13.83 ± 0.09	13.25 ± 0.06	12.52 ± 0.07	12.31 ± 0.08	22.68 ± 0.14	18.75 ± 0.11	16.25 ± 0.10	11.63 ± 0.08
18.5	13.34 ± 0.08	12.46 ± 0.06	11.88 ± 0.06	11.61 ± 0.08	20.24 ± 0.13	17.72 ± 0.11	15.45 ± 0.10	11.08 ± 0.07
19.5	12.71 ± 0.08	11.93 ± 0.06	11.21 ± 0.06	10.83 ± 0.07	18.34 ± 0.12	16.56 ± 0.10	14.56 ± 0.09	10.31 ± 0.07
No of events	450671	922523	771267	483401	518172	547895	531424	502143

Table 1 (continued)

Energy	95 ± 4 MeV	144 ± 3 MeV	194 ± 2 MeV	238 ± 2 MeV	281 ± 2 MeV	311 ± 2 MeV	347 ± 2 MeV	386 ± 2 MeV
Target length	3 cm 5.31 g/cm^2	3 cm 5.31 g/cm^2	3 cm 5.31 g/cm^2	3 cm 5.31 g/cm^2	3 cm 5.31 g/cm^2	3 cm 5.31 g/cm^2	3 cm 5.31 g/cm^2	3 cm 5.31 g/cm^2
Angular resolution	1.355°	0.874°	0.734°	0.651°	0.573°	0.551°	0.517°	0.468°
Up-down consistency $[\chi^2/df]$	0.629	1.431	0.849	1.080	1.129	0.715	1.074	0.751
θ[°]	A_c	A_c	A_c	A_c	A_c	A_c	A_c	A_c
5.5	0.058 ± 0.011	0.239 ± 0.015	0.370 ± 0.018	0.393 ± 0.020	0.379 ± 0.017	0.400 ± 0.018	0.373 ± 0.013	0.391 ± 0.015
6.5	0.104 ± 0.016	0.315 ± 0.015	0.440 ± 0.018	0.438 ± 0.019	0.452 ± 0.017	0.448 ± 0.018	0.432 ± 0.013	0.423 ± 0.015
7.5	0.216 ± 0.018	0.349 ± 0.014	0.465 ± 0.017	0.471 ± 0.019	0.515 ± 0.017	0.500 ± 0.018	0.481 ± 0.014	0.426 ± 0.016
8.5	0.192 ± 0.018	0.344 ± 0.013	0.522 ± 0.017	0.553 ± 0.019	0.530 ± 0.017	0.539 ± 0.018	0.497 ± 0.014	0.468 ± 0.016
9.5	0.210 ± 0.017	0.376 ± 0.013	0.531 ± 0.017	0.562 ± 0.019	0.565 ± 0.017	0.522 ± 0.019	0.508 ± 0.014	0.441 ± 0.017
10.5	0.236 ± 0.017	0.373 ± 0.013	0.569 ± 0.017	0.599 ± 0.019	0.578 ± 0.018	0.565 ± 0.019	0.489 ± 0.015	0.432 ± 0.018
11.5	0.202 ± 0.016	0.412 ± 0.013	0.587 ± 0.017	0.655 ± 0.020	0.574 ± 0.018	0.539 ± 0.020	0.479 ± 0.016	0.392 ± 0.019
12.5	0.211 ± 0.016	0.423 ± 0.013	0.578 ± 0.018	0.583 ± 0.021	0.557 ± 0.019	0.470 ± 0.021	0.428 ± 0.017	0.409 ± 0.020
13.5	0.203 ± 0.016	0.424 ± 0.013	0.614 ± 0.018	0.593 ± 0.021	0.489 ± 0.020	0.471 ± 0.022	0.378 ± 0.017	0.318 ± 0.021
14.5	0.203 ± 0.016	0.448 ± 0.014	0.581 ± 0.019	0.574 ± 0.022	0.422 ± 0.021	0.394 ± 0.023	0.319 ± 0.018	0.284 ± 0.021
15.5	0.195 ± 0.017	0.473 ± 0.015	0.531 ± 0.020	0.498 ± 0.023	0.389 ± 0.021	0.407 ± 0.024	0.318 ± 0.018	0.222 ± 0.022
16.5	0.180 ± 0.017	0.476 ± 0.015	0.539 ± 0.021	0.399 ± 0.024	0.347 ± 0.022	0.281 ± 0.024	0.272 ± 0.019	0.285 ± 0.022
17.5	0.208 ± 0.018	0.455 ± 0.016	0.467 ± 0.021	0.382 ± 0.024	0.301 ± 0.022	0.270 ± 0.024	0.199 ± 0.019	0.244 ± 0.022
18.5	0.221 ± 0.019	0.469 ± 0.017	0.416 ± 0.022	0.363 ± 0.024	0.324 ± 0.022	0.215 ± 0.024	0.226 ± 0.019	0.180 ± 0.022
19.5	0.239 ± 0.020	0.433 ± 0.017	0.402 ± 0.022	0.273 ± 0.025	0.205 ± 0.023	0.230 ± 0.025	0.220 ± 0.019	0.170 ± 0.022
δ_{exp} Data/fit (L) Data/fit (H)	1.011 ± 0.023	0.995 ± 0.009	1.006 ± 0.009	0.998 ± 0.011	0.993 ± 0.010	1.010 ± 0.012 1.009 ± 0.012	0.997 ± 0.010 1.004 ± 0.010	1.001 ± 0.013 1.011 ± 0.013
θ[°]	$d\sigma/d\Omega$	$d\sigma/d\Omega$	$d\sigma/d\Omega$	$d\sigma/d\Omega$	$d\sigma/d\Omega$	$d\sigma/d\Omega$	$d\sigma/d\Omega$	$d\sigma/d\Omega$
5.5	100.00 ± 0.31	100.00 ± 0.43	100.00 ± 0.54	100.00 ± 0.56	100.00 ± 0.50	100.00 ± 0.53	100.00 ± 0.40	100.00 ± 0.45
6.5	35.19 ± 0.17	81.92 ± 0.36	90.74 ± 0.48	89.05 ± 0.49	88.56 ± 0.44	86.70 ± 0.45	85.92 ± 0.34	84.84 ± 0.38
7.5	23.94 ± 0.13	79.20 ± 0.33	84.16 ± 0.43	80.82 ± 0.43	77.00 ± 0.38	74.77 ± 0.39	71.93 ± 0.29	69.49 ± 0.32
8.5	22.24 ± 0.12	77.56 ± 0.31	77.05 ± 0.38	70.85 ± 0.38	65.75 ± 0.33	62.81 ± 0.34	60.41 ± 0.25	57.18 ± 0.27
9.5	21.78 ± 0.11	73.59 ± 0.28	69.81 ± 0.35	62.06 ± 0.34	56.72 ± 0.29	52.95 ± 0.29	50.56 ± 0.21	46.52 ± 0.23
10.5	21.06 ± 0.10	67.53 ± 0.26	61.58 ± 0.31	53.12 ± 0.30	48.28 ± 0.25	44.57 ± 0.26	41.46 ± 0.18	38.14 ± 0.20
11.5	20.33 ± 0.10	61.74 ± 0.23	53.57 ± 0.28	45.81 ± 0.26	40.70 ± 0.22	37.23 ± 0.22	34.01 ± 0.16	31.05 ± 0.17
12.5	18.85 ± 0.09	54.40 ± 0.21	46.32 ± 0.25	39.37 ± 0.23	34.39 ± 0.20	31.33 ± 0.20	28.44 ± 0.14	25.62 ± 0.15
13.5	17.49 ± 0.08	48.35 ± 0.19	40.11 ± 0.22	33.47 ± 0.21	29.77 ± 0.18	27.19 ± 0.18	24.41 ± 0.13	21.89 ± 0.13
14.5	15.85 ± 0.08	41.62 ± 0.17	34.66 ± 0.20	29.34 ± 0.19	25.58 ± 0.16	23.51 ± 0.16	21.30 ± 0.11	19.17 ± 0.12
15.5	14.05 ± 0.07	36.27 ± 0.16	29.76 ± 0.18	25.79 ± 0.17	22.87 ± 0.14	20.85 ± 0.14	19.03 ± 0.10	17.35 ± 0.11
16.5	12.59 ± 0.06	31.49 ± 0.14	26.68 ± 0.16	23.04 ± 0.16	21.02 ± 0.13	18.84 ± 0.13	17.42 ± 0.10	15.98 ± 0.10
17.5	10.99 ± 0.06	26.76 ± 0.13	23.50 ± 0.15	21.07 ± 0.14	18.87 ± 0.12	17.41 ± 0.12	16.09 ± 0.09	14.80 ± 0.10
18.5	9.60 ± 0.05	23.49 ± 0.11	21.42 ± 0.14	19.49 ± 0.14	17.68 ± 0.12	16.60 ± 0.12	15.33 ± 0.09	14.16 ± 0.09
19.5	8.17 ± 0.05	20.41 ± 0.10	19.82 ± 0.13	1[illegible].24 ± 0.13	16.81 ± 0.11	15.49 ± 0.11	14.44 ± 0.08	13.61 ± 0.09
No of events	660462	851752	493816	4[illegible]9028	473049	403172	682041	503088

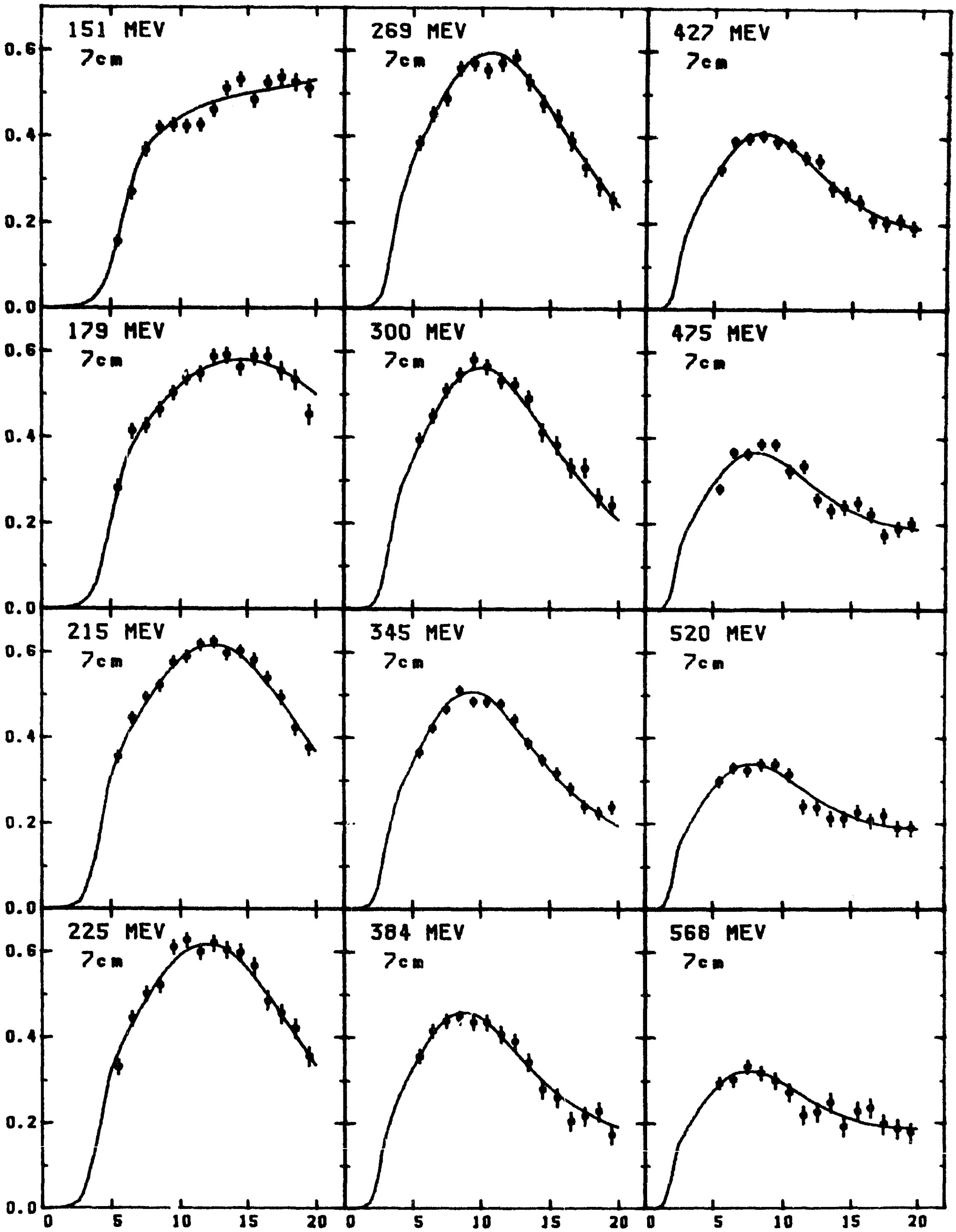

Fig. 2A. The effective proton-carbon analyzing power as a function of the laboratory scattering angle θ. The dots are our experimental points. The full lines show our 7 cm high energy fit (H).

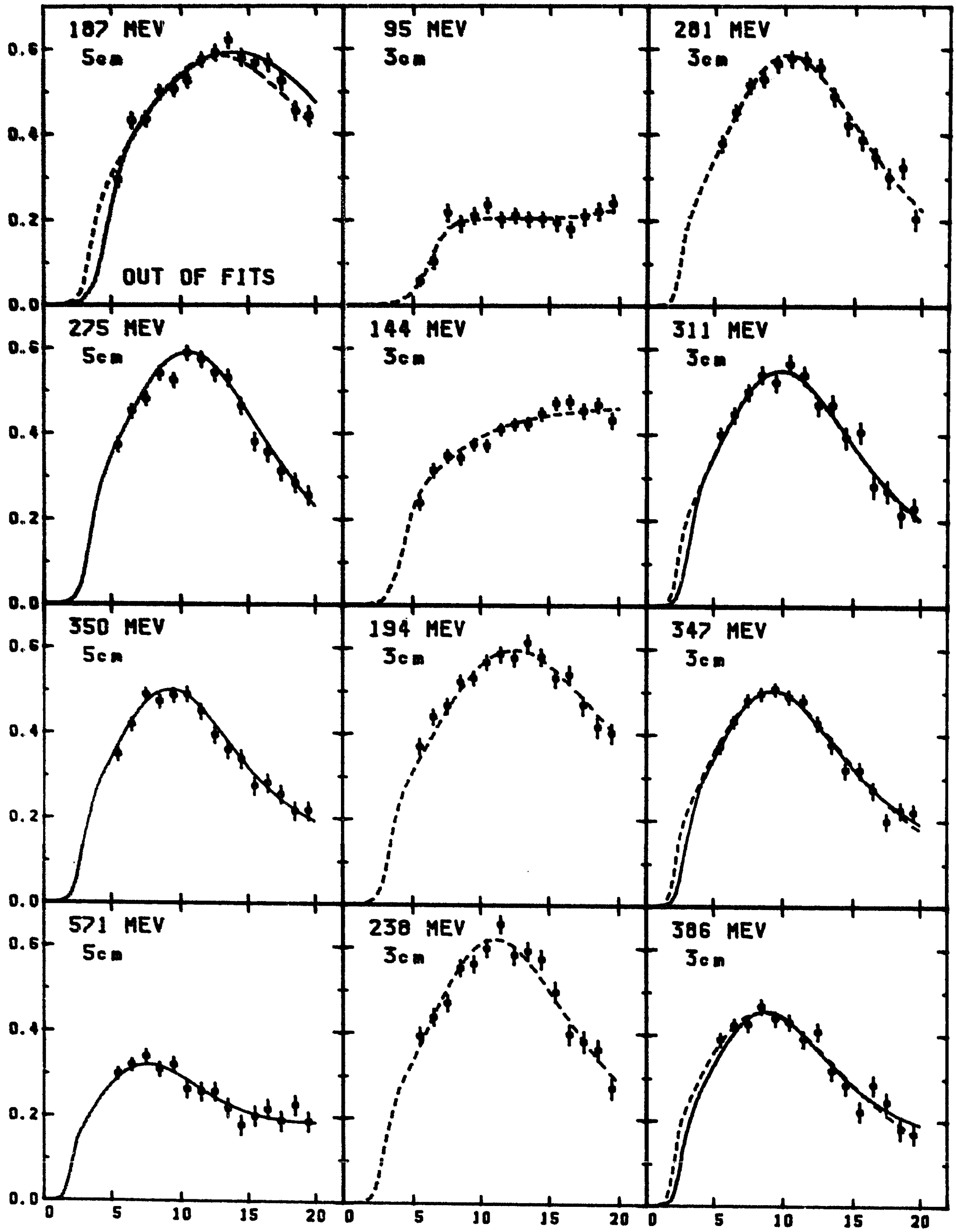

Fig. 2B. The effective proton-carbon analyzing power as a function of the laboratory scattering angle θ. The dots are our experimental points. The full lines show our 7 cm high energy fit (H). Our 3 cm low energy fit (L) is represented by the dotted lines.

Table 2
Results of our angle and energy dependent parametrization of the carbon analyzing power (see section 7).

	"H" fit 7 cm 150–571 MeV $X=\frac{T-400\text{ MeV}}{200\text{ MeV}}$	"L" fit 3 cm 90–386 MeV $X=\frac{T-250\text{ MeV}}{100\text{ MeV}}$
α_0	3.3561	3.6991
α_1	−0.91758	0.26957
α_2	0.38654	−0.0012157
α_3	0.30807	0.17072
β_0	−7.9741	−8.7225
β_1	5.3176	−3.7161
β_2	12.532	12.869
β_3	−3.1091	−2.6088
β_4	–	1.6024
γ_0	857.93	351.97
γ_1	810.41	271.44
γ_2	−127.21	−113.71
γ_3	−163.39	−10.407
γ_4	–	20.331
δ_0	0.079421	–
δ_1	0.12568	–
δ_2	−0.082377	–
C	58.361	75.383
C_0	0.12 [deg.^{2}]	0.12 [deg.^{2}]
C_1	0.38511	0.18472
χ^2/d.f.	1.14	1.17

(2) A low energy fit (denoted by "L") valid for 3 cm target from 90 to 386 MeV. This contains all the present 3 cm data. In addition, we have also included TRIUMF 3 cm data from the BASQUE group [8] between 5° and 20°.

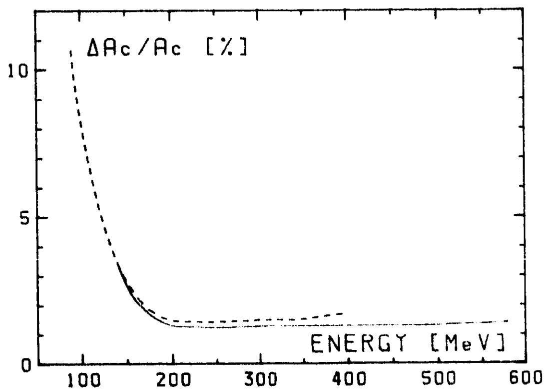

Fig. 3. Percentage uncertainty of our fits. All errors are included. At low energy, the effect of the uncertainty in the beam energy is dominant.

The 5 cm 187 MeV data have not been included in any fits since it was found that target length is significant at this energy.

Fitted parameters are given in table 2. Resulting curves are shown in fig. 2 where solid and dotted lines are used respectively for the "H" and "L" fits. The χ^2 per degree of freedom were 1.14 and 1.29 indicating that the empirical formula adequately describes the data in our angular range. The relative error of our fit (percentage uncertainty of A_c) is shown in fig. 3. Above 170 MeV, it is given mainly by statistical errors and by beam polarization uncertainty (both of the order of 1%). At low energy, the error is dominated by the uncertainty in the beam energy.

In order to check the goodness of our fit at each measured energy, we have computed a deviation factor (δ = data/fit) between the measured data and the fitted formula. This represents the value by which the energy-dependent fit has to be multiplied to give the best adjustment to the data at a particular energy, i.e.,

$$\delta_{exp}=\frac{\sum_\theta w(\theta)\cdot A_{fit}(\theta)\cdot A_{exp}(\theta)}{\sum_\theta w(\theta)A^2_{fit}(\theta)}$$

where $w(\theta)=1/\sigma_\theta^2$ is the statistical weight of an experimental point. The error in δ_{exp} is given by

$$\sigma_\delta^2=1/\sum_\theta w(\theta)A^2_{fit}(\theta),$$

and gives the relative statistical error of the data. Values of δ_{exp} are given in table 1. They are generally well distributed around 1 within their error bars indicating that the relative systematic error introduced by our smoothing stays on the order of 1% at each energy.

In fig. 4 we show the angle-averaged analyzing power A_c as a function of the energy. This average was calculated between 5° and 20° giving equal weight to each angle. The curves are from our formula and the points represent the experimental data included in the fits. As can be seen, the effect of target length appears to be significant.

For the calculation of the average of experimental data we have fixed the angular shape of A_c as given by our fit. The experimental averages are simply calculated by:

$$\bar{A}_{exp}=\delta_{exp}\bar{A}_{fit}$$

This way of computing A_c differs slightly from ref. 10 where the angular shape was adjusted to the data at each energy. Both methods generally give consistent results. Ours has the advantage of allowing comparison of data when the 5°–20° range is not completely covered or when the statistics are poor.

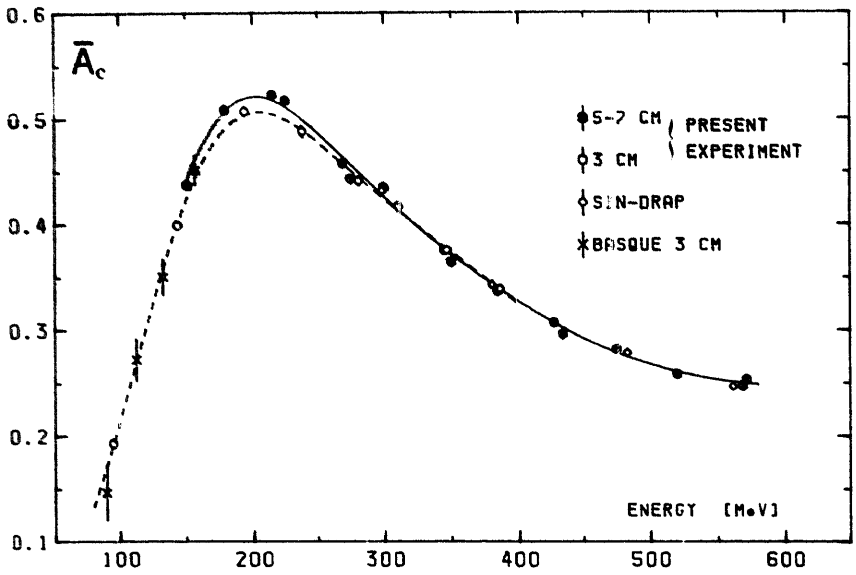

Fig. 4. Angle-averaged effective analyzing power. Curves show our fits. Points are the data included in the fits. Errors are statistical only

8. Comparison with other experiments

Data from different experiments are generally in very good graphical agreement. In order to compare various experiments at different energies, we have computed deviation factors and averages as explained in section 7.

Data from our previous experiment at SIN (DRAP [7]) and BASQUE 3 cm data which were both included in our fits are shown in fig. 4. Other data are shown in

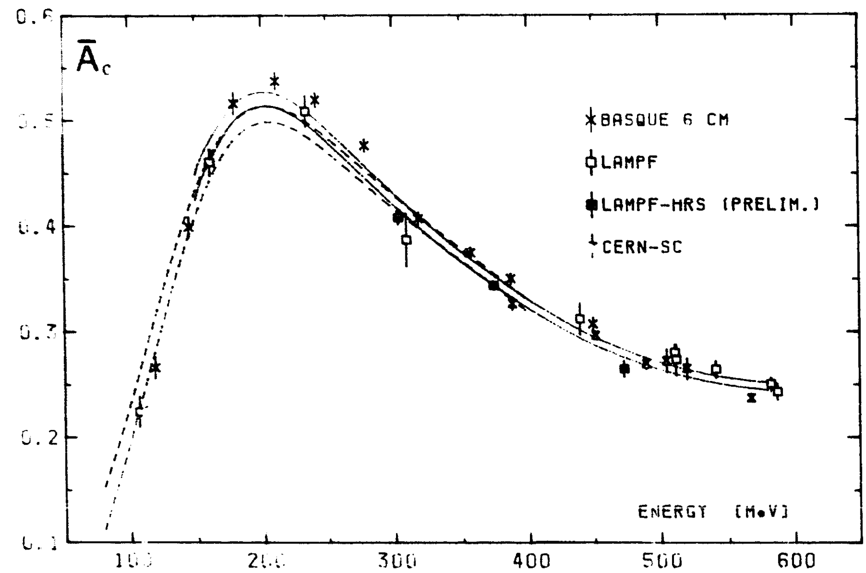

Fig. 5. Angle-averaged effective analyzing power. Curves show the error corridors of our fits. The points come from previous measurements not included in these fits. The errors shown on the points are purely statistical. The angular range is between 5° and 20° (see section 8 for details).

fig. 5 where curves show the error corridors of our fits with all errors included. These data come from our previous experiment at the SC-CERN [9] as well as from TRIUMF (BASQUE 6 cm) [8] and the LAMPF polarimeter [10]. Averages of the preliminary data from LAMPF-HRS were taken from ref. 10.

The data are generally in good agreement with perhaps a small discrepancy above 200 MeV where BASQUE 6 cm data in our angular range are 4% higher than ours as already reported in ref. 10. Recent fits of BASQUE, SIN-DRAP and LAMPF data have also been presented in ref. 10. They are in reasonable agreement with our 7 cm fit.

9. Conclusion

We have presented new precise measurements of the proton–carbon effective analyzing power between 95 and 570 MeV. The data can be reproduced by an energy dependent fit with a relative accuracy of 1–2% above 170 MeV. Reasonable agreement with other available data has been found. At high energy, the effective analyzing power is insensitive to the thickness of the analyzer within statistical accuracy. At low energy however, it can be affected by the target length because of the influence of inelastic events.

A better accuracy would require a considerable effort on systematic effects, especially on the beam polarization calibration. In such a case, comparison between different experiments at low energy would also require a careful study of angular resolution, target length and inelasticity effects as well as effects coming from the strong energy dependence of A_c below 170 MeV.

We would like to thank Prof. D.V. Bugg for supplying the numerical values of the data in ref. 8. We thank SIN and its staff for their technical assistance which was greatly appreciated. This work could not have been done without the aid of the technical staff of our institute. This work was supported by the "Fond National Suisse pour la Recherche Scientifique".

References

[1] E. Aprile et al., Phys. Rev. Lett. 46 (1981) 1047.
[2] R. Hausammann, Thesis 2038, University of Geneva (1982).
[3] E. Aprile-Giboni et al., Phys. Rev. D27 (1983) 2600.
[4] D. Besset et al., Phys. Rev. D21 (1980) 580;
D. Rapin, Thesis 1884, University of Geneva (1979).
[5] D. Besset et al., Nucl. Instr. and Meth. 184 (1981) 365.
[6] V. Hungerbuhler et al., Nucl. Instr. and Meth. 137 (1976) 189.
[7] D. Besset et al., Nucl. Instr. and Meth. 166 (1979) 379.
[8] G. Waters et al., Nucl. Instr. and Meth. 153 (1978) 401.
[9] D. Aebischer et al., Nucl. Instr. and Meth. 124 (1975) 49.
[10] R.D. Ransome et al., Nucl. Instr. and Meth. 201 (1982) 315.